Texture and Tempered Condition Combined Effects on Fatigue Behavior in an Al-Cu-Li Alloy

An Wang, Zhiyi Liu, Meng Liu, Wenting Wu, Song Bai, and Rongxian Yang

Texture and tempered condition combined effects on fatigue behavior in an Al-Cu-Li alloy have been investigated using tensile testing, cyclic loading testing, scanning electron microscope (SEM), transmission electron microscopy (TEM) and texture analysis. Results showed that in near-threshold region, T4-tempered samples possessed the lowest fatigue crack propagation (FCP) rate. In Paris regime, T4-tempered sample had similar FCP rate with T6-tempered sample. T83-tempered sample exhibited the greatest FCP rate among the three tempered conditions. 3% pre-stretching in T83-tempered sample resulted in a reducing intensity of Goss texture and facilitated T_1 precipitation. SEM results showed that less crack deflection was observed in T83-tempered sample, as compared to other two tempered samples. It was the combined effects of a lower intensity of Goss texture and T_1 precipitates retarding the reversible dislocation slipping in the plastic zone ahead the crack tip.

1. Introduction

The major advantages of Al-Li alloys are low density, high stiffness and compatibility with existing metal working facilities (Ref 1). It has been found that addition of 1% lithium to aluminum reduces the density up to 3% and increases modulus by 6% (Ref 2-4). However, alloy exhibits erratic behavior when Li exceeds a certain level. The previous generation of Al-Li alloys, such as 2090, 8090 and 2091 alloys (Ref 5-7), showed serious mechanical anisotropy. Due to the poor fracture toughness in short transverse orientation, some unpredictable problems would happen in manufacturing process. Hence the third-generation alloy with an increased Cu/Li ratio, such as C489 alloy (Ref 8), was developed. However, the elongation of C489 alloy in peak aging condition was too low. 2099 alloy with higher elongation was therefore developed by reducing Li content and increasing Zr content.

In Al-Cu-Li system, there are lots of precipitates, such as δ' (Al$_3$Li), θ' (Al$_2$Cu) and T_1 (Al$_2$CuLi) (Ref 9-11). The δ' Phase is completely coherent with matrix as spherical particle (Ref 12) and has a small mismatch to parent phase, with only 0.08% lattice distortion. The spherical δ' phase can be cut by dislocations, and the dislocation is effortless to slip on a common crystal, rather than cross-slip caused by other phases. Due to the coplanar slip, dislocations will accumulate on grain boundaries, increasing the stress concentration,

inducing crack initiation and crack propagation along slip planes or grain boundaries. The θ' phase is elevated aging product, dissolving out disk-like on {001}$_\alpha$ plane, which has a certain reinforcement effect. The hexagonal T_1 phase is the main strengthening phase in Al-Cu-Li system (Ref 13). It tends to precipitate on the dislocations and grain boundaries, with strong reinforcement effect (Ref 14), which increases the stacking fault energy of δ' phase and reduces the coplanar slip.

The precipitate types, the grain structures, including its size and orientation, play an important role in fatigue crack propagation (FCP) of aluminum alloys. Some researchers, such as Venning (Ref 15) and Estrin (Ref 16), have studied the grain size effect on FCP, yet their results did not always suggest grain refining could give rise to increasing FCP resistance. Zhai et al. (Ref 17) discovered that short fatigue cracks could not extend on the boundary of Goss {011}⟨100⟩, but could easily get through Brass in 8090 alloy. Zhong et al. (Ref 18) investigated the relationship among microscopic structure of 2A97 alloy and the early fatigue crack initiation as well as propagation. Their results showed that the fatigue crack initiated mainly at inclusions on the surface and the coarse second phase in 2A97 alloy. On the other hand, Jata et al. (Ref 19) researched the FCP and fracture toughness of Al-Li-Cu alloy. Experimental results of fatigue crack near the threshold region showed that the irregularity of FCP path and fracture surface could improve the fatigue growth resistance. However, few documents focused on how the microstructure affected the fatigue performance of Al-Cu-Li alloy. Different tempered conditions of Al-Cu-Li alloy were accomplished in this work with a purpose to reveal the microstructure and texture influence on the fatigue test performance.

2. Materials and Methods

The commercial Al-Cu-Li alloy plate was used in present work. The chemical composition of the studied alloys was 2.7 wt.% Cu, 1.78 wt.% Li, 0.7 wt.% Zn, 0.09 wt.% Zr and

An Wang, Zhiyi Liu, Meng Liu, Wenting Wu, Song Bai, and **Rongxian Yang**, Key Laboratory of Non-ferrous Materials, Ministry of Education, Central South University, Changsha 410083, China; and School of Materials Science and Engineering, Central South University, Changsha 410083, China. Contact e-mail: liuzhiyi@mail.csu.edu.cn.

Table 1 Details of the aging treatment of Al-Cu-Li alloy

Temper	Aging treatment parameter
T4	Natural aging
T6	121 °C/12 h + 152 °C/48 h
T83	3%pre-stretching + 121 °C/ 12 h + 152 °C/48 h

Table 2 Tensile properties of the studied Al-Cu-Li alloy

	T4	T6	T83
Tensile strength (MPa)	413 ± 2	474 ± 2	534 ± 1
Yield strength (MPa)	297 ± 1	399 ± 2	512 ± 1
Elongation (%)	19.6 ± 0.1	10.9 ± 0.1	8.9 ± 0.1

Fig. 1 FCP rates, *da/dN*, as a function of ΔK of T4, T6 and T83 tempers

balance Al. The alloy plate was hot rolled to 2.5 mm sheet, then solution treated at 543 °C for 40 min in a salt bath furnace, water quenched and then experienced different aging treatments shown in Table 1. The tensile test was performed on a CSS-44100 universal testing machine with a cross-head speed of 2 mm/min. Mechanical properties reported in present work were the average values of three specimens for each condition. CT specimens were prepared from the sheets in the L-T orientation with a size (in mm) of $45.6 \times 38 \times 2$ (L × W × B). The fatigue crack propagation test was performed on an Instron S810 fatigue testing machine. Fatigue fracture was investigated by FEI Quanta 200 scanning electron microscope. Transmission electron microscopy (TEM) analysis was performed on a Tecnai G^2 20 machine operating at 200 kV. TEM samples were thin disks with 3 mm in diameter and electro-polished by using twin-jet equipment with a voltage of 15 V in an 80% methanol and 20% nitric acid at approximately −20 °C. Texture analysis was observed on a Bruker D8 Discover x-ray diffractor. The (111), (200) and (220) pole figures were measured by the Schulz back-reflection method using Cu K_α radiation. The orientation distribution functions (ODFs) were calculated from the incomplete pole figures using the series expansion method ($l_{max} = 16$) (Ref 20).

3. Results and Discussions

3.1 Mechanical Properties

Tensile test results in Table 2 show that the tensile strength (σ_b), yield strength ($\sigma_{0.2}$) and elongation of T4 sample were, respectively, 413, 297 MPa and 19.6%, and those of T6 sample reached 474, 399 MPa and 10.9%, and those of T83 sample increased to 534, 512 MPa and 8.9%. It was apparent that the samples in T83 temper possessed a higher strength and a lower elongation as compared to those of T4 and T6 tempers.

Figure 1 shows the FCP curves of Al-Cu-Li alloy in various aging conditions. In fatigue Stage I, the FCP rate of natural aging was lowest. In Paris regime, the FCP rates of three conditions were different. The FCP rate of T4 sample increased rapidly, which was slightly higher than that in T6 condition. However, T83 sample exhibited higher FCP rates than that of T4 and T6 tempers. The FCP rates accelerated dramatically at high ΔK regime. T83 sample showed the highest FCP rate and
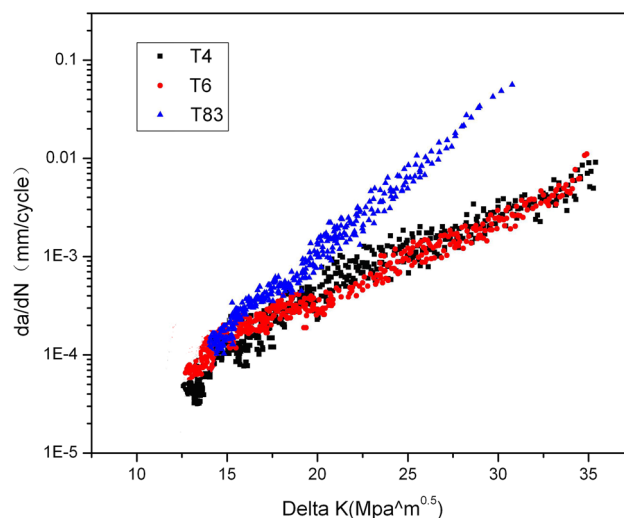
began to fracture when ΔK reached 30 MPa·m$^{0.5}$. Both T4 and T6 samples revealed a similar FCP rate at high ΔK regime.

3.2 Microstructural Characterization

The fractographs of fatigue fracture surfaces in Stage I of all samples showed transgranular fractures, as seen in Fig. 2. The fatigue fracture of T4 temper had many small shear planes, and adjacent planes were connected by tearing ridge. Numerous small shear planes are shown in Fig. 2(b) and (c). In Stage I, crack propagation mainly originated from plane shears. The sizes of FCP planes were different in various tempers because of diverse plastic deformation between matrix and slip bands.

The fatigue fracture in Stage I was transgranular fractures, and crack propagation generated fatigue striations in Paris stage. Figure 3 shows that fatigue striations were composed of numerous parallel wave crooked streaks, which were also vertical to the FCP direction. The finer fatigue striations suggested the lower FCP rates and higher FCP resistance. Similarly, the fatigue striations in T4 and T6 tempers were fine, which increased obviously in T83 temper, and was consistent with FCP curves in Fig. 1. There are some secondary cracks in Fig. 3(a) and (b). Secondary cracks made the crack propagation path complex, thus reducing driving force of fatigue crack extension and contributing to the low FCP rates in T4 and T6 tempers.

Figure 4 shows TEM micrographs of different aging conditions. Selected area electron diffraction (SAED) pattern in the top right corner in Fig. 4(a) shows diffraction spots $1/2\{220\}_\alpha$ of δ′ precipitates. Small and dispersed δ′ precipitates in matrix corresponded to white dots. The δ′ precipitate was completely coherent with matrix and could be cut by dislocations leading to high plasticity. However, a mass of δ′ precipitates would give rise to coplanar slip, thereby reducing the strength. In Fig. 4(b), needle-like θ″ and θ′ precipitates separated out from $[100]_\alpha$ and $[001]_\alpha$ directions in addition to the δ′ precipitates. Meanwhile, diffraction spots $1/2\{001\}_\alpha$ in Fig. 4(b) reveal the presence of θ′ precipitates. The θ′ precipitate was semi-coherent to matrix and could reduce coplanar slip, increasing strength distinctly. As seen from the diffraction spots $1/3\{111\}_\alpha$ and $2/3\{210\}_\alpha$ in Fig. 4(c), a mass of T_1 and some S′ precipitates have dissolved out in T83

temper. Moreover, T_1 phase is relative to $[110]_\alpha$ direction and S′ phase is relative to $[152]_\alpha$ and $[512]_\alpha$ directions. Figure 4(c) shows a dark-field TEM micrograph of T83 sample, in which a mass of δ′ precipitates and some long δ′/θ′ composites were observed. Therefore, δ′, β′, θ′, T_1 and S′ phases coexisted in T83 temper. The plasticity was low but the strength increased.

As shown in Fig. 4, there were lots of fine δ′ precipitates and small amount of θ″ precipitates in T4 temper. However, the sizes of δ′ precipitates in T6 temper increased obviously, with

some θ″ and θ′ precipitates in matrix. In T83 temper, a mass of thick needle-like T_1 precipitates was present in matrix. The δ′ precipitate possessed the high elasticity modulus, which could decrease opening displacement of the crack tip. On the other hand, existence of δ′ precipitates resulted in local inhomogeneous deformation and crack deflection. Thus, the crack propagation path became complex. Dominant T_1 precipitates could reduce the coplanar slip of δ′ precipitates in T83 temper, retarding the reversible dislocation slipping in the plastic zone ahead the crack
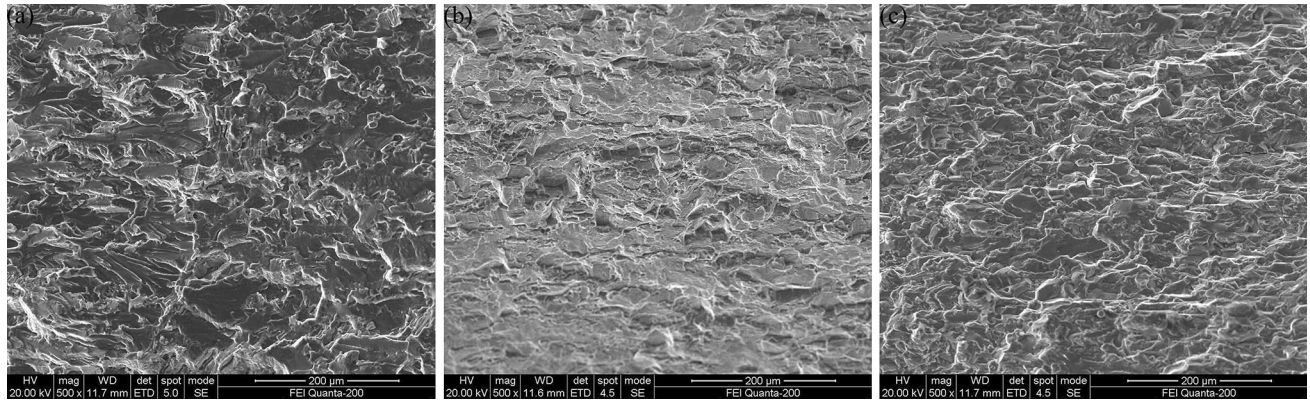

Fig. 2 SEM fractographs showing the fatigue surfaces of three different treatments (ΔK = 9.3 MPa·m$^{0.5}$) (a) T4; (b) T6; (c) T83
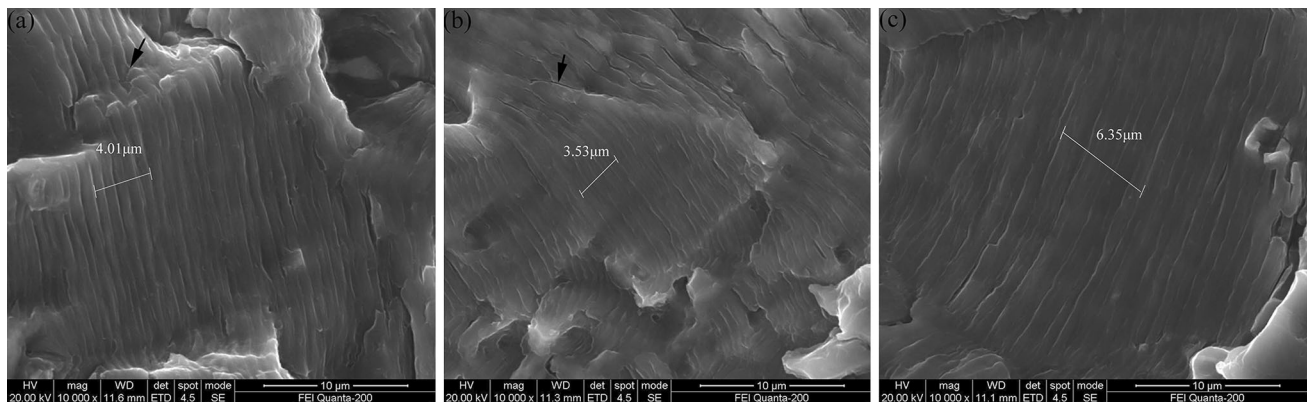
Fig. 3 Fatigue striation appearance of three different treatments (ΔK = 19.5 MPa·m$^{0.5}$) (a) T4; (b) T6; (c) T83
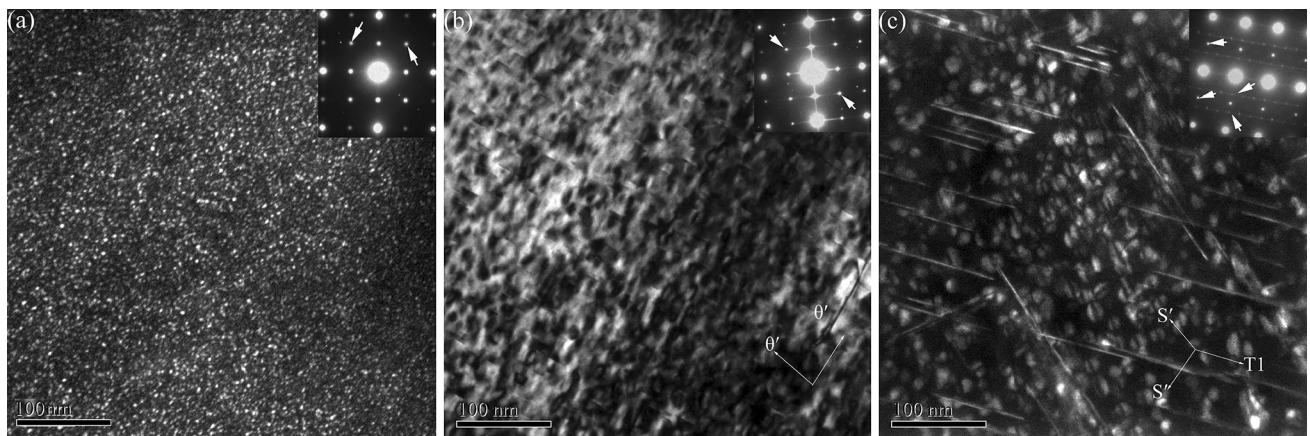
Fig. 4 TEM images and corresponding SAED patterns of the samples after different treatments. (a) DF image of $[100]_\alpha$ zone axis in T4 condition; (b) BF image of $[100]_\alpha$ zone axis in T6 condition; (c) DF image of $[112]_\alpha$ zone axis in T83 condition
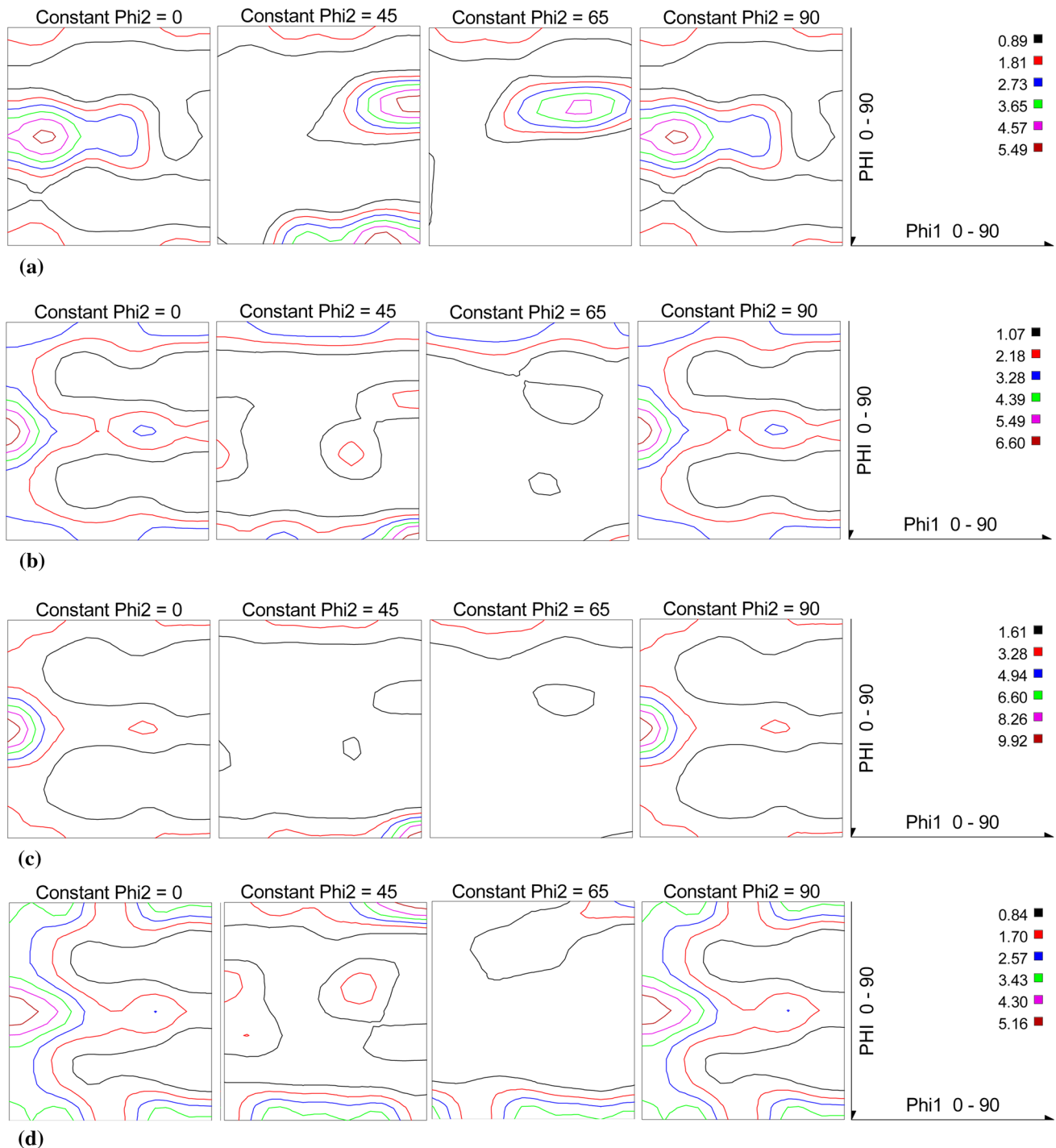
**Fig. 5** Texture measurement results after different treatments (a) hot rolling; (b) T4; (c) T6; (d) T83

tip. Lewandowska (Ref 21) studied the effect of precipitates on fatigue life in Al-Li-Zr alloy. The fatigue life of Al-Li-Zr alloy was related to the precipitate size. The sizes of δ' precipitates in different samples were different. The size of δ' precipitates was 2 nm after natural aging, became 8 nm after 200 °C/2 h and reached 20 nm after 200 °C/24 h. Results showed that stress cycles of natural aging temper doubled that of 200 °C/2 h aged temper in Al-Li-Zr alloy. According to the extensive studies (Ref 22), the increasing size of δ' precipitates leads to distinct stress concentration and was detrimental to fatigue life. In this work, δ' precipitates were fine after natural aging, but became coarse in T6

temper. However, similar fatigue properties of T4 and T6 tempers indicated that it was not precipitates but other factors affected the fatigue property of the studied Al-Cu-Li alloy.

3.3 Texture Analysis

The ODF sections illustrated the texture in Al-Cu-Li alloy after hot rolling was mainly composed by Goss ($\{011\}\langle111\rangle$) with strength level up to 5.49, Copper ($\{211\}\langle111\rangle$) with strength level of 5.49, S with strength level of 4.57, and weaker Cube and Brass, as shown in Fig. 5(a). The texture of T4 temper in
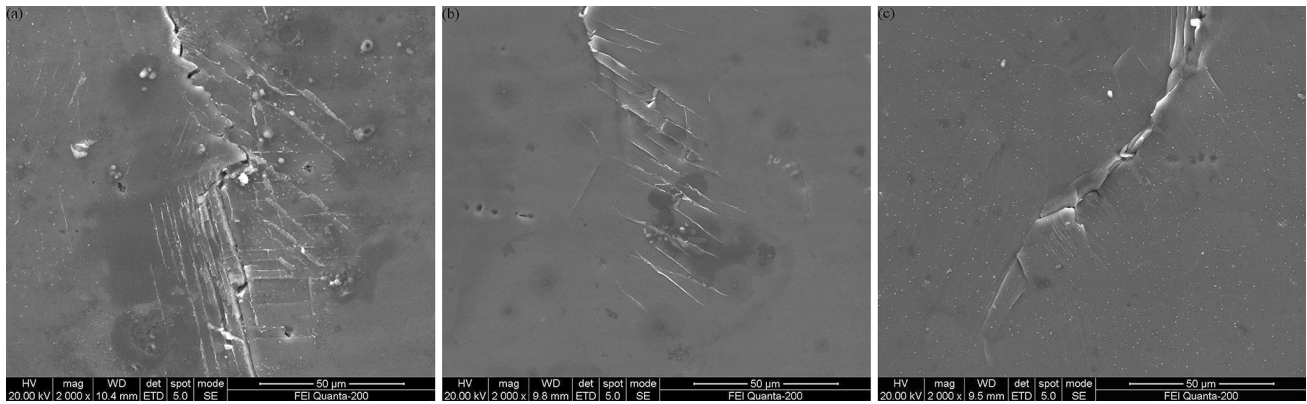
Fig. 6 Crack-tip slip band after different treatments (a) T4; (b) T6; (c) T83
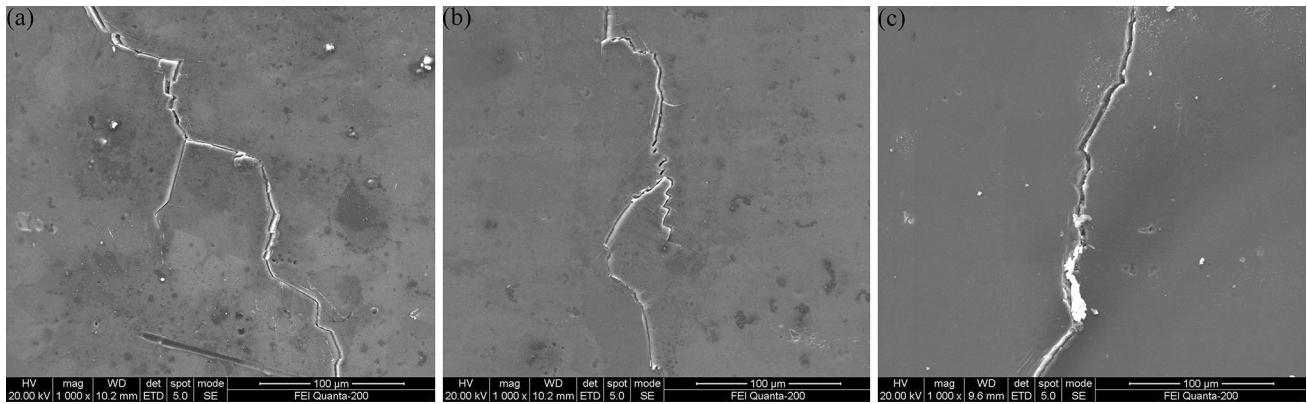
Fig. 7 Crack deflection of FCP stage I after different treatments (a) T4; (b) T6; (c) T83

Fig. 5(b) was dominated by Goss having strength level of 6.6 and Cube with strength level of 3.28. Weak Copper component was also detected. The texture of T6 temper was mainly composed of Goss with strength level of 9.92 and a little of Cube, as shown in Fig. 5(c). The texture of T83 condition in Fig. 5(d) was mainly composed of Goss with strength level of 5.16, Brass with strength level of 3.43 and Copper with strength level of 3.43. Comparisons of Fig. 5(b), (c), and (d) show the highest strength level of Goss was T6 temper and that of T83 was the lowest one.

The effect of textures on fatigue crack propagation resistance of aluminum alloy has been well investigated. In addition to the investigation of Zhai et al. (Ref 17), Liu et al. (Ref 23) studied FCP in fatigue Stage II, revealing $\{001\}\langle100\rangle$ Goss gives rise to a great fatigue crack deflection. The result showed that compared with $\{001\}\langle110\rangle$ Cube and $\{001\}\langle100\rangle$ Cube + $\{011\}\langle211\rangle$ Brass, the sample containing $\{011\}\langle100\rangle$ Goss + $\{001\}\langle100\rangle$ Cube possessed the greatest FCP resistance. However, the sample containing $\{001\}\langle100\rangle$ Goss + $\{011\}\langle211\rangle$ Brass possessed the highest FCP rate. The intensity of $\{011\}\langle100\rangle$ Goss in T6 temper was highest, so the FCP rate was low. Nevertheless, T83 temper contained weaker $\{011\}\langle100\rangle$ Goss but stronger $\{011\}\langle211\rangle$ Brass, finally leading to the highest FCP rate.

3.4 Fatigue Crack Propagation

At the initial stage of FCP, fatigue cracks propagated along the direction of 45° with tensile stress, forming slip bands that were parallel to the crack, as shown in Fig. 6(a). However, the size of crack propagation deformation zone was smaller than that of grains, like shape Z. Textures greatly affected crack propagation. Because the orientation of adjacent grains was different, crack propagation would deflect to other planes which were in favor of propagation when getting through grain boundaries, improving FCP resistance. Due to the texture of T4 temper was mainly composed by $\{011\}\langle100\rangle$ Goss, the fatigue crack in Fig. 7(a) deflected to different angles, with second crack existence, enhancing the FCP resistance. This also took place in T6 temper, as shown in Fig. 7(b). However, deflected angle of fatigue crack decreased obviously in T83 temper. Secondary cracks were also seldom observed in Fig. 7(c). Thus the FCP resistance was considerably degraded in T83 temper.

With the expansion of the fatigue crack, it extended from Stage I to Stage II (Paris regime). The mechanism of fatigue crack extension changed from pure shear mechanism to double sliding mechanism, as shown in Fig. 6(b). Fatigue striations are typical in Stage II. A lot of theoretical models explain the formation of fatigue crack and planar extension in Paris regime. The plastic passivation model by Larid et al. (Ref 24) was widely accepted. With the lower FCP resistance, the distance of crack propagation was greater. So the width of fatigue striation could reflect the value of FCP rates. The fatigue striation widths of T4 and T6 tempers were narrower than that of T83 temper, indicating the FCP rate of T4 and T6 tempers was slower than that of T83 temper.

4. Conclusions

1. T4-tempered Al-Cu-Li alloy possessed the lowest strength, the highest ductility and FCP resistance, while T83 (3%pre-stretching + 121 °C/12 h + 152 °C/48 h)-tempered alloy possessed the highest strength, the lowest ductility and FCP resistance.
2. The FCP rates of T4 and T6 tempers were quite similar. Besides, T83 temper reveals the highest FCP rate. This was attributed to the combined influence of the precipitates and textures.
3. $\{011\}\langle100\rangle$ Goss grains induced fatigue crack deflection and was responsible for the enhanced FCP resistance. Besides, T_1 precipitate retarded the reversible dislocation slipping in the plastic zone ahead the crack tip, leading to less crack deflection and greater FCP rate.

Acknowledgment

References

1. D.C. Vander Kooi, W. Park, and M.R. Hilton, Characterization of Cryogenic Mechanical Properties of Aluminum-Lithium Alloy C-458, *Scr. Mater.*, 1999, **41**(1), p 1185–1190
2. R.J. Rioja and J. Liu, Evolution of Al-Li Base Products for Aerospace and Space Application, *Metall. Mater. Trans. A*, 2012, **43**(1), p 3325–3337
3. A. Heinz, A. Haszler, C. Keidel, S. Moldenhauer, R. Benedictus, and W.S. Miller, Recent Development in Aluminum Alloys for Aerospace Applications, *Mater. Sci. Eng., A*, 2000, **280**(1), p 102–107
4. K.T. Venkateswara Rao and R.O. Ritchie, Fatigue of Aluminum-Lithium Alloys, *Int. Mater. Rev.*, 1992, **37**(1), p 153–185
5. E.J. Lavernia, T.S. Srivatsan, and F.A. Mohamed, Strength, Deformation, Fracture Behaviour and Ductility of Aluminum-Lithium Alloys, *J. Mater. Sci.*, 1990, **25**(2), p 1137–1158
6. P. Giomiero, Y. Brechet, F. Louchet et al., Microstructure and Mechanical Properties of a 2091 Al-Li Alloy-II: Mechanical Properties: Yield Stress and Work Hardening, *Acta Metall. Mater.*, 1992, **40**(1), p 857–861
7. C. Giummarra, R.J. Rioja, Gh. Bray, et al, Al-Li Alloys: Development of Corrosion Resistant, High Toughness Aluminum-lithium Aerospace Alloys, in *Proceedings of ICAA11 Conference*, Aachen, Germany, 2008, 1(1), p 176–188
8. K.S. Kumar and F.H. Henbaum, The Effect of Li Content on the Natural Aging Response of Al-Cu-Li-Mg-Ag-Zr Alloys, *Acta Mater.*, 1997, **45**(1), p 2317–2327
9. R. Yoshimura, T.J. Konno, E. Abe et al., Transmission Electron Microscopy Study of the Early Stage of Precipitations in Aged Al-Li-Cu Alloys, *Acta Mater.*, 2003, **51**(1), p 2891–2903
10. S.P. Ringer, B.C. Muddle, and I.J. Polmear, Effects of Cold Work on Precipitation in Al-Cu-Mg-(Ag) and AL-Cu-Li-(Mg-Ag) Alloy, *Metall. Mater. Trans. A*, 1995, **26**(1), p 1659–1671
11. J.I. Pérez-Landazabal, M.L. Nó, G. Madariage, V. Recarte, and J.S. Juan, Quantitative Analysis of δ′ Precipitation Kinetics in Al-Li Alloys, *Acta Mater.*, 2000, **48**(1), p 1283–1296
12. C.S. Tsao, C.Y. Chen, T.Y. Kuo et al., Size Distribution and Coarsening Kinetics of δ' Precipitates in Al-Li Alloys Considering Temperature and Concentration Dependence, *Mater. Sci. Eng., A*, 2003, **363**(1), p 228–233
13. F.W. Gayle, F.H. Heubaum, and J.R. Pickens, Structure and Properties During Aging of an Ultra-High Strength Al-Cu-Li-Ag-Mg Alloy, *Scr. Metall. Mater.*, 1990, **24**(1), p 79–84
14. S.C. Wang and M.J. Starink, Precipitates and Intermetallic Phases in Precipitation Harding Al-Cu-Mg-(Li) Based Alloys, *Int. Mater. Rev.*, 2005, **50**(4), p 203–204
15. L. Venning, S.C. Hogg, I. Sinclai, and I.A.S. Reed, Fatigue Crack Growth and Closure in Fine-Grained Aluminium Alloys, *Mater. Sci. Eng., A*, 2006, **128**(1), p 247–255
16. Y. Estrin and A. Vinogradov, Fatigue Behaviour of Light Alloys with Ultrafine Grain Structure Produced by Severe Plastic Deformation, *Int. J. Fatigue*, 2010, **32**(1), p 898–907
17. T. Zhai, X.P. Jiang, J.X. Li, M.D. Garratt, and G.H. Bray, The Grain Boundary Geometry for Optimum Resistance to Growth of Short Fatigue Cracks in High Strength Al-Alloy, *Int. J. Fatigue*, 2005, **27**(1), p 1202–1209
18. J. Zhong, S. Zhong, Z.-Q. Zheng, H.-F. Zhang, and X.-F. Luo, Fatigue Crack Initiation and Early Propagation Behavior of 2A97 Al Li Alloy, *Trans. Nonferr. Met. Soc. China*, 2014, **24**(1), p 303–309
19. K.V. Jata and E.A. Starke, Fatigue Crack Growth and Fracture Toughness Behavior of an Al-Li-Cu Alloy, *Metall. Mater. Trans. A*, 1986, **17**(6), p 1011–1026
20. H.J. Bunge, *Texture Analysis in Materials Science*, Butterworths-Heinemann, London, 1982
21. M. Lewandowska, J. Mizera, and J.W. Wyrzykowski, Cyclic Behaviour of Model Al-Li Alloys: Effect of the Precipitates State, *Mater. Charact.*, 2000, **45**(1), p 195–202
22. B.M. Gable, A.W. Zhu, A.A. Csontos, and E.A. Starke, The Role of Plastic Deformation on the Competitive Microstructural Evolution and Mechanical Properties of a Novel Al-Li-Cu-X Alloy, *J. Light Met.*, 2001, **1**(1), p 1–14
23. Z. Liu, F. Li, P. Xia, S. Bai, G. Yanxia, Y. Dier, and S. Zeng, Mechanisms for Goss-Grains Induced Crack Deflection and Enhanced Fatigue Crack Propagation Resistance in Fatigue Stage II, of an AA2524 Alloy, *Mater. Sci. Eng., A*, 2015, **625**(1), p 271–277
24. C. Laird and G.C. Smith, Crack Propagation in High Stress Fatigue, *Philos. Mag.*, 1962, **7**(77), p 847–857